Optimization of the backing material of a low frequency PVDF detector for ion beam monitoring during small animal proton irradiation

J. Lascaud, R. Kowalewski, B. Wollant, H. Carmigniani, K. Schnürle, P. Dash, H.-P. Wieser, J. Bortfeldt, R. Kalunga, R. Rouffaud, A. Gérard, M. Vidal, J. Hérault, D. Certon and K. Parodi

©2021 IEEE. Personal use of this material is permitted. Permission from IEEE must be obtained for all other uses, in any current or future media, including reprinting/republishing this material for advertising or promotional purposes, creating new collective works, for resale or redistribution to servers or lists, or reuse of any copyrighted component of this work in other works.

Cite as: J. Lascaud *et al.*, "Optimization of the backing material of a low frequency PVDF detector for ion beam monitoring during small animal proton irradiation," 2021 IEEE International Ultrasonics Symposium (IUS), 2021, pp. 1-4, doi: 10.1109/IUS52206.2021.9593703.

Optimization of the backing material of a low frequency PVDF detector for ion beam monitoring during small animal proton irradiation

Julie Lascaud*§, Rafal Kowalewski*, Benjamin Wollant*, Henri Carmigniani*, Katrin Schnürle*, Pratik Dash*, Hans-Peter Wieser*, Jonathan Bortfeldt*, Ronaldo Kalunga*, Rémi Rouffaud†, Anaïs Gérard‡, Marie Vidal‡, Joël Hérault‡, Dominique Certon† and Katia Parodi*§

*Ludwig-Maximilians-Universität München, Garching b. Munich, Germany
†GREMAN UMR 7347 Université de Tours, CNRS, INSA Centre Val de Loire, 37071 Tours Cedex 2, France
‡Centre Antoine Lacassagne - Fédération Claude Lalanne, 227 avenue de Lanterne, Nice

§ Email: j.lascaud@physik.uni-muenchen.de and katia.parodi@physik.uni-muenchen.de

***Abstract*—This study investigates the use of PVDF sensors for the detection of low pressure kHz thermoacoustic signals, emanating from pulsed proton beams during small animal irradiation. In particular, the impact of the backing material and detector geometry on the measured signal amplitude and accuracy of time-of-flight estimations is assessed. A simulation model, including FLUKA Monte Carlo simulations of the proton dose, pressure propagation using k-Wave, modeling the backing geometry and a Mason model of the PVDF electroacoustic response is proposed. Thereafter, suitable backing materials are investigated by varying the backing density, the speed of sound and the detector geometry. Tungsten is found to be a good candidate to improve the sensor sensitivity, while maintaining accurate localization of the maximum of the proton dose, i.e., Bragg peak localized with an error lower than $5\,\%$ for the considered scenarios. Tungsten backing as thin as $2.5\,\mathrm{mm}$ allows to improve the sensitivity of the detector by a factor 4 compared to $10\,\mathrm{mm}$ epoxy backing.**

***Index Terms*—PVDF, ionoacoustics, thermoacoustics, proton range verification**

I. Introduction

Accelerated ion beams allow for a well-localized irradiation of the tumor volume, resulting in a better sparing of healthy tissues compared to other forms of external beam radiatiotherapies [1]. Improvement of the treatment effectiveness relies, among other methods, on small animal studies, to understand the influence of the treatment strategy (e.g., spatial and temporal distribution of the therapeutic dose) on the biological response. The more localized irradiation offered by accelerated ions, or protons in the context of this study, comes at the cost of a greater sensitivity on the stopping position of the proton beam (Bragg peak, BP). Therefore, any misalignment of the small animal or changes of its anatomy from one treatment fraction to the other, in addition to intrinsic uncertainties in the determination of the tissue stopping power, may compromise the treatment plan and understanding of its therapeutic outcomes [2], [3]. Consequently, full reliability of preclinical studies on small animals, and their scalability to clinical cases, require precise irradiation, including image guidance and treatment monitoring to visualize the delivered dose (energy deposited by unit of mass) within the daily anatomy. This can be achieved by a co-registration of anatomical images (e.g., from ultrasound images or X-ray computed tomography) with the detection of thermoacoustic waves resulting from the sharp energy deposition of pulsed ion beams (thereafter referred to as ionoacoustics) [4], [5]. In ideal conditions, assuming instantaneous dose deposition and homogeneous medium, the initial pressure resulting from the energy deposited by a proton beam stopped in a given medium directly relates to the three dimensional dose distribution and medium properties, i.e., density and so-called Grüneisen parameter [6]. In these ideal conditions, the initial pressure reaches its maximum at the BP position, where the dose is maximum as well. As a result, positioning an acoustic detector along the proton beam axis, distal to the BP, allows to verify the proton beam range in the medium by a time-of-flight analysis, whereas the initial pressure distribution can be reconstructed using multiple sensors [7], both requiring the use of broadband detection system to accurately capture the shape of the ionoacoustic signal in which the information of the dose is imprinted [8]. This study investigates the use of a $28\,\mu\mathrm{m}$-thick PVDF detector, operating at frequencies much lower than its thickness-mode resonance frequency ($34\,\mathrm{MHz}$ in air), enabling the broadband detection of low-pressure ($\leq 0.1\,\mathrm{Pa}$) and low-frequency ($\leq 100\,\mathrm{kHz}$) ionoacoustic signals at clinically relevant dose [9]. Particular attention is paid to the sensor dimensions and material budget, which should be minimized in order to be integrated in a small animal proton irradiator without interfering with the other foreseen imaging modalities [10].

II. Methodology

A. Simulation workflow and model validation

Fig.1(a) shows the simulation workflow employed for this study and validated during experiments at the Centre Antoine Lacassagne (Nice, France). The proton dose ($D(\boldsymbol{r})$) was computed in 3D using the FLUKA Monte Carlo code [11], [12], and converted to an initial pressure $p_0(\boldsymbol{r})$, knowing the medium density ($\rho(\boldsymbol{r})$) and Grüneisen parameter ($\Gamma(\boldsymbol{r})$), as described in eq. 1 [9].

$$p_0(\boldsymbol{r}) = \Gamma(\boldsymbol{r}) \cdot D(\boldsymbol{r}) \cdot \rho(\boldsymbol{r}) \tag{1}$$

The initial pressure, medium properties (density, speed of sound and Grüneisen parameter) were defined through a dedicated Python routine and input to the C++ code of the k-Wave toolbox [13], using in this way the k-space pseudo-spectral time-domain model for the propagation of the ionoacoustic pressure. The pressures were recorded and averaged on a surface corresponding to the sensor surface, and its exact geometry (including the backing material) and composing materials were systematically included in the k-Wave simulations to account for the reflection at the sensor interface and potential wave interference inside the detector backing. The averaged pressure was thereafter convolved with a $3\,\mu s$ Gaussian pulse mimicking realistic proton pulse time profile [9], and subsequently convolved with the open-circuit sensitivity of the PVDF detector obtained from a Mason model.

Fig.1(b) illustrates the experimental and simulation setup used for the model validation. A silicone rubber phantom ($\rho = 1020\,\mathrm{kg\,m^{-3}}$, $\Gamma = 0.58$, and $v = 997\,\mathrm{m\,s^{-1}}$) immersed in water was irradiated by a clinical pulsed proton beam at several energies from $171.58\,\mathrm{MeV}$ to $174.08\,\mathrm{MeV}$ and a proton beam intensity of $0.7\,\mathrm{nA}$ with a repetition rate of $1\,\mathrm{kHz}$, corresponding to 4.37×10^6 protons/pulse. The ionoacoustic signals were measured with an in-house detector ($1\,\mathrm{cm}^2$ rectangular PVDF; $1\,\mathrm{cm}$-thick epoxy backing), amplified by $60\,\mathrm{dB}$ using a low-noise amplifier (HVA-10M-60-B, FEMTO Messtechnik GmbH, Germany) and acquired using a digital oscilloscope (6404D PicoScope, Pico Technology Ltd., GB). All the measurements were averaged over 1000 acquisitions to improve the signal-to-noise ratio, allowing for better comparison with the noise free simulations. Fig.1(c) demonstrates the good agreement between the simulated and experimental signals. The signal amplitude (related to the sensor sensitivity) is properly modeled. The slight discrepancies in the signal shape may be attributed to inaccurate model of the clinical beam and distortions induced by the noise which are not take into account in our simulation workflow.

B. PVDF backing optimization

The model was employed to investigate the influence of the backing on the detection of ionoacoustic emissions in a mouse-like silicone rubber phantom ($4\,\mathrm{cm}$ diameter half-cylinder), the simulation setup is represented in Fig.2(a). For these simulations, a $100\,\mathrm{MeV}$ proton beam (lowest energy

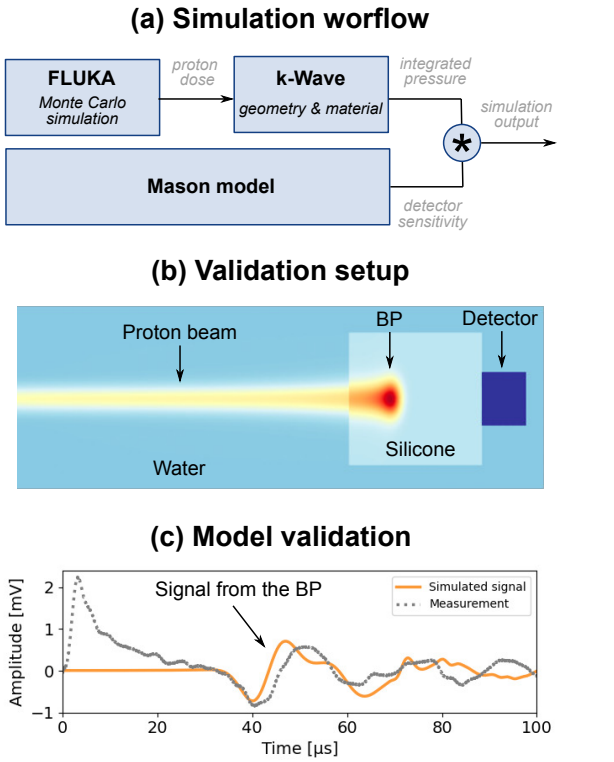

Fig. 1. Simulation workflow and model validation: (a) schematic representation of the simulation workflow, (b) schematic top view of the experimental and simulation setup used for the model validation, and (c) comparison between the simulated ionoacoustic signal (orange) and experiments (gray) for a $173.58\,\mathrm{MeV}$ clinical pulsed proton beam.

clinically available at the accessible synchro-cyclotron facility) was considered. The proton beam was degraded by a $63\,\mathrm{mm}$-thick PMMA range shifter to reduce the proton beam range in the phantom down to $6.84\,\mathrm{mm}$. The beam diameter was also reduced by using a $7\,\mathrm{mm}$-thick brass collimator with a $2\,\mathrm{mm}$ aperture, positioned in between the range shifter and the irradiated phantom. The same proton beam intensity as for the experiments was considered (4.37×10^6 protons/pulse). The silicone phantom was maintained in air and the acoustic coupling between the sensor and the phantom was ensured by a $1\,\mathrm{mm}$-thick water layer. In the first part of the simulation study, the width of the square sensor was fixed to $5\,\mathrm{mm}$ and the backing density and speed of sound were varied. The detector was positioned in the computational grid such that its back side was in contact with a perfectly match layer, avoiding spurious reflections in the backing material. The second part of the investigation was focused on the impact of the detector geometry (sensor width and backing thickness) on the measured ionoacoustic signal for tungsten backing ($\rho_{tungsten} = 19\,300\,\mathrm{kg\,m^{-3}}$ and $v_{tungsten} = 5200\,\mathrm{m\,s^{-1}}$). Air was introduced behind the detector, allowing for reflection in the backing material. For all the simulations, the detector sensitivity and accuracy of the ionoacoustic BP localization were evaluated. The sensitivity was assessed from the peak-to-peak amplitude of the signal directly propagating from

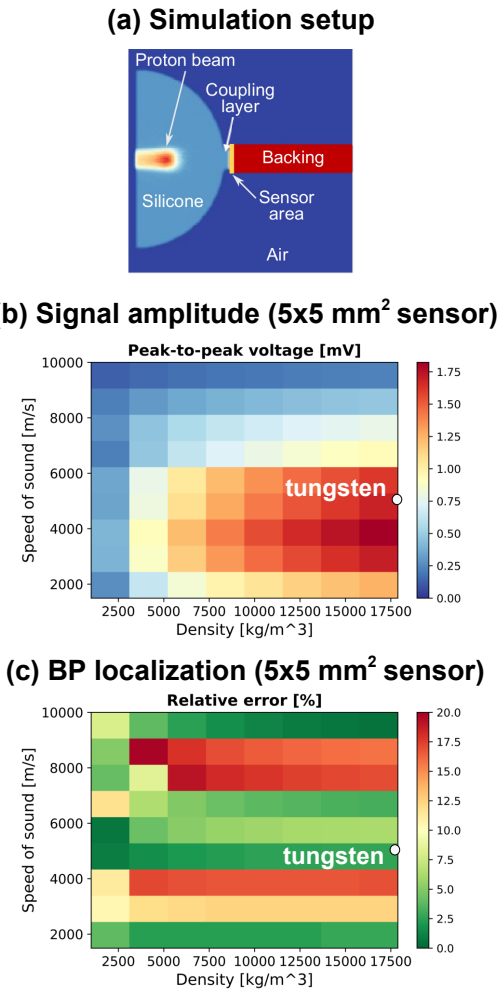

Fig. 2. Influence of the backing properties on the measured ionoacoustic signal: (a) schematic representation of the simulation setup, (b) evolution of the signal peak-to-peak amplitude as a function of the backing density ans speed of sound, and (c) evolution of the relative error on the Bragg peak localization estimated from the signal time-of-flight as a function of the backing density ans speed of sound. The white dot indicates the position of tungsten backing on the density and speed of sound maps.

the BP, whereas the relative error on the BP localization was determined from a time-of-flight estimation. The time-of-flight was defined as the time difference between $50\,\%$ of the rising edge of the Gaussian pulse (proton pulse) and the first maximum of the signal absolute value. These criteria were chosen to minimize the localization error based on the known Bragg peak position.

III. Results and Discussion

A. Optimal semi-infinite backing

The evolution of the signal amplitude and BP localization error as a function of the backing properties (density and speed of sound) are showed in Fig.2(b,c), respectively, for semi-infinite backing (backing thickness $\gg$ signal wavelength, here equal to $14\,\mathrm{mm}$ in silicone). For the considered densities and speeds of sound, the sensitivity increases with the backing density. For a given density, the signal reaches its maximum of amplitude for speeds of sound ranging from $2500\,\mathrm{m\,s^{-1}}$ to $6000\,\mathrm{m\,s^{-1}}$, and decreases for higher speeds of sound. The error on the BP localization mostly depends on the speed of sound in the backing material. For the considered arrangement and using a $5\,\mathrm{mm}$ by $5\,\mathrm{mm}$ sensor, the lowest error are obtained for speed of sound ranging from $4000\,\mathrm{m\,s^{-1}}$ to $6000\,\mathrm{m\,s^{-1}}$, or speeds of sound lower than $2000\,\mathrm{m\,s^{-1}}$ or higher than $9000\,\mathrm{m\,s^{-1}}$. It should be noted that, varying the sensor width changes the optimal speed of sound in the backing, which seems to highlight a contribution of the lateral wave propagation in the backing on the time-of-flight estimation. Based on these results, tungsten appears to be a good candidate as a backing material, allowing for sensitive and accurate ionoacoustic detection in case on semi-infinite backing.

B. Tungsten backing with a finite thickness

Fig.3(c,d) shows the evolution of the signal amplitude and error on the BP localization in case of tungsten backing for different sensor widths and backing thicknesses. The results are compared to epoxy backing previous used (Fig.3(a,b)). In general, for the investigated sensor geometries, larger sensing areas and thicker backings are favorable to high detected amplitudes (Fig.3(a,c)). For both backing materials, the peak-to-peak amplitude mostly depends on the sensor width and is less sensitive to the backing thickness. No clear pattern emerges for the error on the BP localization, which tends to be lower for the smallest sensor widths and backing thicknesses (Fig.3(b,d)). Further study should investigate more in detail the influence of the lateral wave propagation in the backing by disentangling the width of the sensor element from the lateral dimension of the detector. Optimal backing design is found using a $2.5\,\mathrm{mm}$-thick tungsten backing with a width of $10\,\mathrm{mm}$, leading to a peak-to-peak amplitude of $1.9\,\mathrm{mV}$ and a localization error of $4.4\,\%$. Such a backing allows to reduce by a factor 4 the sensor space requirement compared to the prototype we used previously, and increases the detector sensitivity by almost a factor 2 for a similar accuracy on the BP localization.

IV. Conclusion

In this study we investigated PVDF sensors for the detection of kHz thermoacoustic signals emanating from pulsed proton beams during small animal irradiation. In particular, we assessed the impact of the backing material and detector geometry on the measured signal amplitude and accuracy of time-of-flight estimations, aiming to minimize the sensor dimension and maximize the sensitivity and accuracy of the Bragg peak localization. A simulation model, including FLUKA Monte Carlo simulations of the proton dose, pressure propagation using k-Wave, modeling the backing geometry and a Mason model of the PVDF electroacoustic response was developed and validated during experiments at a clinical proton facility. Thereafter, the density and speed of sound of semi-infinite backings were varied in-silico on a broad range, in order

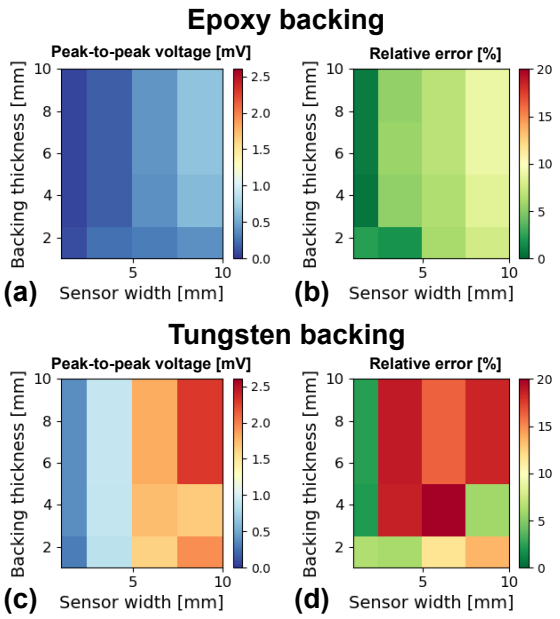

Fig. 3. Influence of backing geometry on the measured ionoacoustic signal for epoxy backing (a) evolution of the signal peak-to-peak amplitude as a function of the sensor width and backing thickness, (c) evolution of the relative error on the Bragg peak localization estimated from the signal time-of-flight as a function of the sensor width and backing thickness, and for backing made of tungsten: (c) evolution of the signal peak-to-peak amplitude, and (d) relative error on the Bragg peak localization as a function of the sensor width and backing thickness.

to define suitable backing materials. Tungsten was found to be a good candidate to improve the sensor sensitivity, while maintaining accurate localization of the proton dose maximum, i.e., Bragg peak localized with an error lower than 5 %. Finally, the sensor width and backing thickness were varied, using either an epoxy or tungsten backing material. For similar Bragg peak localization accuracy, tungsten backing allows simultaneously to reduce the thickness of the detector and to increase its sensitivity. The proposed PVDF sensor design is foreseen to be integrated in a small animal irradiation platform, for which further work is required to assess the impact of such a backing material on the other imaging modalities.

Acknowledgment

The authors acknowledge financial support from the European Research Council (SIRMIO, Grant 725539), BayFrance (Grant FK312019), the European Commission (ATTRACT, Grant 777222) and the Centre for Advanced Laser Applications. The authors would like to thank Édi Liang for his support in the preparation of the final simulations.

References

[1] D. R. Olsen, Ø. S. Bruland, G. Frykholm, and I. N. Norderhaug, "Proton therapy–a systematic review of clinical effectiveness," *Radiotherapy and oncology*, vol. 83, no. 2, pp. 123–132, 2007.

[2] B. Schaffner and E. Pedroni, "The precision of proton range calculations in proton radiotherapy treatment planning: experimental verification of the relation between ct-hu and proton stopping power," *Physics in Medicine & Biology*, vol. 43, no. 6, p. 1579, 1998.

[3] H. Paganetti, "Range uncertainties in proton therapy and the role of monte carlo simulations," *Physics in Medicine & Biology*, vol. 57, no. 11, p. R99, 2012.

[4] S. Kellnberger, W. Assmann, S. Lehrack, S. Reinhardt, P. Thirolf, D. Queirós, G. Sergiadis, G. Dollinger, K. Parodi, and V. Ntziachristos, "Ionoacoustic tomography of the proton bragg peak in combination with ultrasound and optoacoustic imaging," *Scientific reports*, vol. 6, p. 29305, 2016.

[5] S. Patch, M. K. Covo, A. Jackson, Y. Qadadha, K. Campbell, R. Albright, P. Bloemhard, A. Donoghue, C. Siero, T. Gimpel *et al.*, "Thermoacoustic range verification using a clinical ultrasound array provides perfectly co-registered overlay of the bragg peak onto an ultrasound image," *Physics in Medicine & Biology*, vol. 61, no. 15, p. 5621, 2016.

[6] K. Parodi and W. Assmann, "Ionoacoustics: A new direct method for range verification," *Modern Physics Letters A*, vol. 30, no. 17, p. 1540025, 2015.

[7] J. Lascaud, P. Dash, H.-P. Wieser, R. Kalunga, M. Wuerl, W. Assmann, and K. Parodi, "Investigating the accuracy of co-registered ionoacoustic and ultrasound images in pulsed proton beams," *Physics in Medicine & Biology*, vol. 66, no. 18, p. 185007, 2021.

[8] J. Lascaud, R. Kalunga, S. Lehrack, H.-P. Wieser, F. S. Englbrecht, M. Würl, W. Assmann, A. S. Savoia, and K. Parodi, "Applicability of capacitive micromachined ultrasonic transducers for the detection of proton-induced thermoacoustic waves," in *2019 IEEE International Ultrasonics Symposium (IUS)*. IEEE, 2019, pp. 143–146.

[9] K. C. Jones, C. M. Seghal, and S. Avery, "How proton pulse characteristics influence protoacoustic determination of proton-beam range: simulation studies," *Physics in Medicine & Biology*, vol. 61, no. 6, p. 2213, 2016.

[10] K. Parodi, W. Assmann, C. Belka, J. Bortfeldt, D.-A. Clevert, G. Dedes, R. Kalunga, S. Kundel, N. Kurichiyanil, P. Lämmer *et al.*, "Towards a novel small animal proton irradiation platform: the sirmio project," *Acta Oncologica*, vol. 58, no. 10, pp. 1470–1475, 2019.

[11] T. Böhlen, F. Cerutti, M. Chin, A. Fassó, A. Ferrari, P. Ortega, A. Mairani, P. Sala, G. Smirnov, and V. Vlachoudis, "The FLUKA Code: Developments and Challenges for High Energy and Medical Applications," *Nuclear Data Sheets*, vol. 120, no. 0, pp. 211 – 214, 2014.

[12] A. Ferrari, P. R. Sala, A. Fassó, and J. Ranft, "FLUKA: a multi-particle transport code," *CERN-2005-10*, vol. INFN/TC_05/11, SLAC-R-773, 2005.

[13] B. E. Treeby and B. T. Cox, "k-wave: Matlab toolbox for the simulation and reconstruction of photoacoustic wave fields," *Journal of biomedical optics*, vol. 15, no. 2, p. 021314, 2010.